ISSN 0030-400X, Optics and Spectroscopy, 2014, Vol. 117, No. 5, pp. 769–783. © Pleiades Publishing, Ltd., 2014.

CONDENSED-MATTER SPECTROSCOPY

Optical Properties of Rare Earth Doped Strontium Aluminate (SAO) Phosphors: A Review[1]

D. S. Kshatri and A. Khare

Department of Physics, National Institute of Technology, Raipur 492010, Chhattisgarh, India

e-mail: akhare.phy@nitrr.ac.in

Received March 18, 2014

Abstract—After the first news on rare earth (RE) doped strontium aluminate (SAO) phosphors in late 1990s, researchers all over the world geared up to develop stable and efficient persistent phosphors. Scientists studied various features of long lasting phosphors (LLP) and tried to earmark appropriate mechanism. However, about two decades after the discovery of $SrAl_2O_4$: Eu^{2+}, Dy^{3+}, the number of persistent luminescent materials is not significant. In this review, we present an overview of the optical characteristics of RE doped SAO phosphors in terms of photoluminescence (PL), thermoluminescence (TL) and afterglow spectra. Also, we refresh the work undertaken to study diverse factors like dopant concentration, temperature, surface energy, role of activator, etc. Simultaneously, some of our important findings on SAO are reported and discussed in the end.

DOI: 10.1134/S0030400X14110101

INTRODUCTION

In last decade nano-scale materials have revolutionized the research all over the world because of their potential impact in many fields such as photonics, electronics, sensing, and catalysis [1]. These materials offer large number of applications in the areas of organic solar cells, carbon nanotubes, solid state batteries, fuel cells, super plastic ceramics, multifunctional materials, molecular electronics, single electron devices, biosensors, and lasers [2], etc. Such materials take advantages of size-induced changes in structural, optical and electronic properties to create enhanced luminescent materials, whose properties differ from the corresponding bulk phase [3]. Out of these, the ones suited as phosphor host material show considerable size dependent luminescence properties when an impurity is doped in a quantum-confined structure. The impurity incorporation transfers the dominant recombination route from the surface states to impurity states. If the impurity-induced transition can be localized as in the case of the transition metals or the RE elements, the radiative efficiency of the impurity induced emission increases significantly. The emission and decay characteristics of the phosphors are, therefore, modified in nanocrystallized form. Also, the continuous shift of the absorption edge to higher energy due to quantum confinement effect, imparts these materials a degree of tailorability. Obviously, all these attributes of a doped nanocrystalline phosphor material are very attractive for optoelectronic device applications. Nanoparticles, in general, are supposed to have nearly half of their atoms contained in top two monolayers, which make optical properties highly sensitive to surface morphology. Blue shift of band gap and strong non-linear response of nanoparticles of CdS and CdSe in glass samples were first reported [4] in the early 1980s. Enhanced quantum properties were further confirmed with study of other semiconductor nanoparticles of ZnS, PbS, ZnSe and CdSe [5]. Metal nanoparticles [6] were also synthesized with a view to prepare better catalysts. The size has to be less than twice of Bohr radii of exciton (3–5 nm) for quantum confinement regime.

Persistent luminescence is an optical phenomenon, whereby a material is excited with high energy radiation and the resulting visible luminescent emission remains visible for an appreciable time from seconds to many hours after the excitation has stopped. The effect is also called phosphorescence, afterglow, or long lasting phosphorescence (LLP). As follows, the long afterglow is governed by the slow liberation of trapped charge carriers by thermal excitation. Therefore, the process can be influenced by changing the temperature. Often, thermoluminescence (TL) is used as a diagnostic method for determining trap levels. The phenomenon of persistent luminescence has been known to mankind for over a thousand years [7]. The phenomenon of persistent luminescence was not researched much till the end of the 20th century. In the following years pure and doped zinc sulfide (ZnS) was the most famous and widely used persistent phosphor [8]. However, its properties like brightness and lifetime were quite low for practical purposes. This problem was solved by introducing radioactive elements such as promethium or tritium in the powders to stimulate the brightness and lifetime of the light emission [9]. Still a

[1] The article is published in the original.

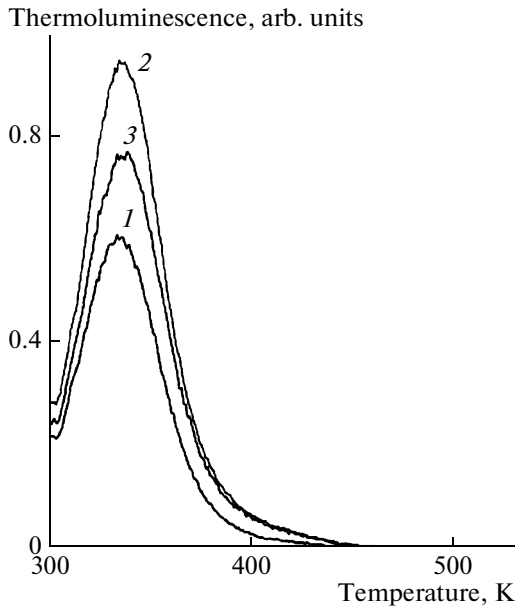

Fig. 1. TL Glow curves of $SrAl_2O_4$: Eu^{2+}, Dy^{3+} excited by photons of different wavelengths: 425 (*1*), 400 (*2*), 350 nm (*3*), and recorded at a heating rate of 5 K/s.

commercial glow in the dark object had to contain a large amount of luminescent material to yield an acceptable afterglow.

After the discovery of a new phosphor $SrAl_2O_4$: Eu^{2+}, Dy^{3+} with LLP [10], the aluminates have been the center of attraction in persistent luminescent research with a large number of publications. The alkaline earth aluminates MAl_2O_4 (M = Ca, Sr, Ba) are the most studied family of long lasting persistent luminescent materials. The bright-green luminescence of the monoclinic [11] $SrAl_2O_4$: Eu^{2+} was discovered [12] and described two years later with $CaAl_2O_4$: Eu^{2+} and $BaAl_2O_4$: Eu^{2+} [13]. It shows a considerable afterglow, suggesting that the existence of co-dopants is not imperative to obtain persistent luminescence [14].

Different methods are employed to synthesize co-doped MAl_2O_4: Eu^{2+} in an efficient and cheaper way. The solid-state reaction technique, where sample is treated at 1300–1400°C, is the most commonly used method to obtain the desired compound. On the other hand, laser heated pedestal growth [15], sol–gel [16], microwave route [17], Pechini method [18] and combustion [19] methods are proven to be successful. However, it is worth noting that not all the techniques lead to identical crystallographic and luminescent properties. $SrAl_2O_4$: Eu^{2+}, Dy^{3+} prepared by microwave synthesis shows a decreased initial brightness of the afterglow, together with a small blue shift of the emission spectrum, possibly due to the small grain size [17]. A similar blue shift is reported for sol–gel prepared $SrAl_2O_4$: Eu^{2+}, Dy^{3+} [20]. During the preparation of $CaAl_2O_4$ by combustion or a sol–gel method, Holsa and coworkers [21] obtained an unusual hexagonal crystal structure instead of the expected monoclinic one [22]. Other researchers produced grains with orthorhombic structure [23]. It is clear that utmost care should be taken while comparing luminescence of compounds prepared with different procedures. The exact composition of the starting mixture has important consequences for the afterglow behavior. A deficit of alkaline earths usually enhances the afterglow [24], while an excess of barium in $BaAl_2O_4$: Eu^{2+}, Dy^{3+} can annihilate the persistent luminescence completely [25]. This paper reviews the latest developments and research work carried out in the field of LLP. We have also tried to compare the results of photoluminescence (PL) and TL for RE doped SAO phosphors synthesized through various techniques. Also, we discuss the effect of dopant concentration, temperature dependence, effect of surface energy, role of activator, etc.

NOTEWORTHY CONTRIBUTION IN THE FIELD OF SAO PHOSPHORS

Spectroscopic Study of Persistent TL

In order to understand the mechanism of persistent luminescence, the location of the relevant lanthanide ground state energies with respect to the valence band and the conduction band of the host compound is crucial. While moving through the lanthanide series from Ce towards Lu, it has been established that the absolute location of the lanthanide ground state varies in a systematic fashion and is almost independent of the type of compound. To predict the location of all other states, one only requires information on the ground state level location of a few lanthanide ions. Dorenbos [26] in his recent publication proposed schemes for $Sr_2MgSi_2O_7$, $SrAl_2O_4$, and $CaGa_2S_4$ based on an alternative model. Bos and his co-workers [27] reported a versatile new facility to study photoionization processes in impurity doped compounds and the detailed TL and PL studies on $SrAl_2O_4$: Eu^{2+}, Dy^{3+} phosphors. Figure 1 shows selected TL glow curves of $SrAl_2O_4$: Eu^{2+}, Dy^{3+} powder phosphor following optical excitation at 350, 400, and 425 nm whereas Fig. 2 shows the TL excitation spectrum (TLES) of $SrAl_2O_4$: Eu^{2+}, Dy^{3+} at room temperature (RT) obtained by integration of all measured glow curves in the temperature interval 300–400 K and also the PL excitation spectrum (PLES) of Eu^{2+} emission at 10 K. At this temperature the long persistent luminescence was strongly suppressed. The PLES of the Eu^{2+} $5d$–$4f$ emission starts at around 475 nm, rises steeply to the maximum around 425 nm, and falls off for lower wavelengths before showing a second maximum at 363 nm. The TLES starts at the same wavelength but shows a grad-

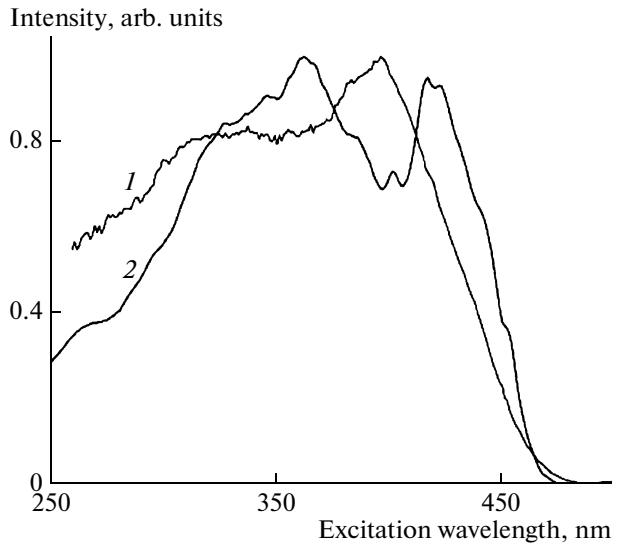

Fig. 2. TL (*1*) and PL (*2*) excitation spectra of $SrAl_2O_4$: Eu^{2+}, Dy^{3+}.

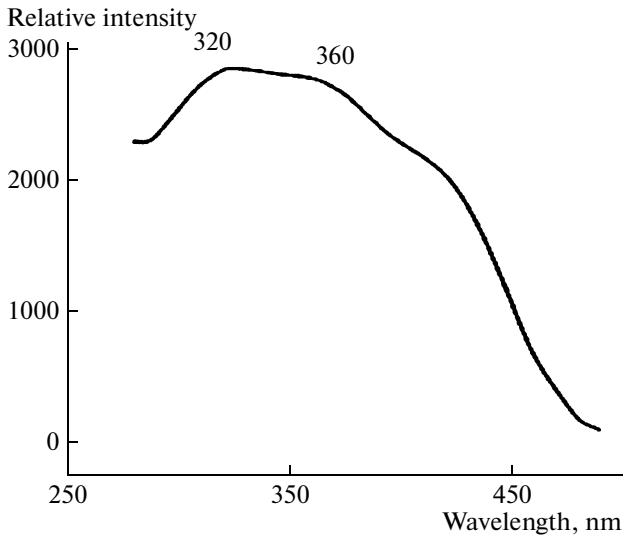

Fig. 3. Excitation spectra of the sample prepared through solid state reaction technique.

ual increase in intensity with shorter wavelengths until a maximum is reached. It is clear that there are differences between the TL and PL spectra but the most important observation is that the onset of the PLES coincides with the onset of the TLES. This observation is a strong indication that excitation of Eu^{2+} leads to trap filling, which is the first step in the persistent luminescence mechanism [28].

Effect of Surface Energy

A growing interest in $SrAl_2O_4$: Eu, Dy, a kind of long afterglow luminescent materials, has been reported extensively [29]. Since it has good luminescent properties such as suitable emission color, no radiation, high initial luminescent intensity and long lasting time, which may reach 16 h [10], $SrAl_2O_4$: Eu, Dy will be widely used in the near future. For most of luminescent materials, the luminescent properties are greatly dependent on the grain size. When the grain size reaches nanometer grade, the luminescent materials exhibit some attractive properties, such as the blue shift of excitation and emission spectra [2].

Tang et al. [30] prepared $SrAl_2O_4$: Eu, Dy phosphor using gel method. Compared with samples prepared by solid state reactions, the grain size of the gel method was greatly reduced to nanometer grade. A clear blue shift occurred in the excitation and emission spectra of nano $SrAl_2O_4$: Eu, Dy, of which the peak of the excitation and emission spectra are found to he at 323 and 500 nm, respectively. The brightness of nano $SrAl_2O_4$: Eu, Dy was found to reduce greatly. The blue shift and the change of luminescent intensity in nano $SrAl_2O_4$: Eu, Dy materials was attributed to the effect of surface energy. The samples prepared through solid state reaction and sol–gel method were sintered at 1380°C. Figures 3 and 4 respectively show the excitation and emission spectra of samples prepared through solid state reaction at 1380°C (Solid-1380). The phosphor sample reaches a maximum at 320 and 360 nm in excitation spectra and exhibits a broad band peak at 520 nm in emission spectra. However, in the sample prepared through gel method at 1380°C (Gel-1380), although the excitation and emission spectra, as shown in Figs. 5 and 6 have a similar shape to Solid-1380, both of them shift towards low wavelength side of the spec-

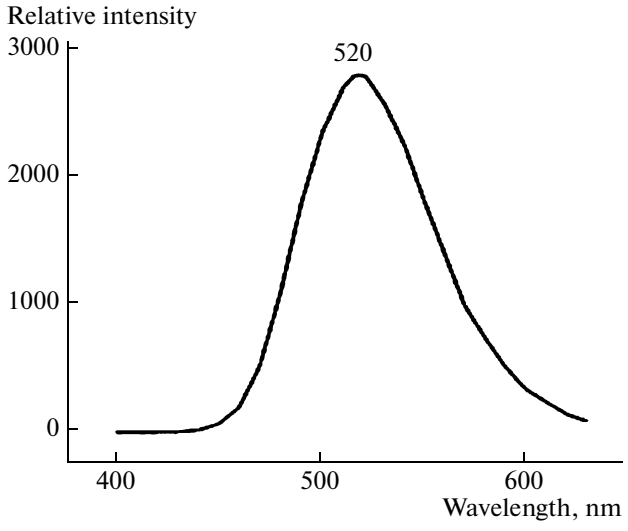

Fig. 4. Emission spectra of the sample prepared through solid state reaction technique.

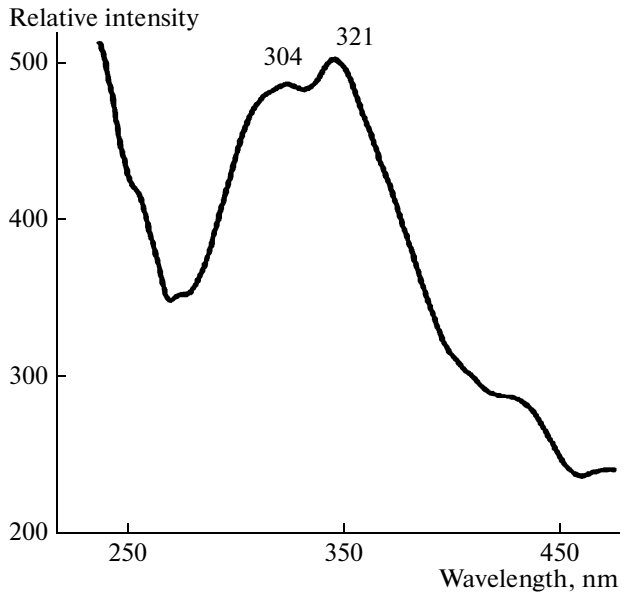

Fig. 5. Excitation spectra of the sample prepared through gel technique.

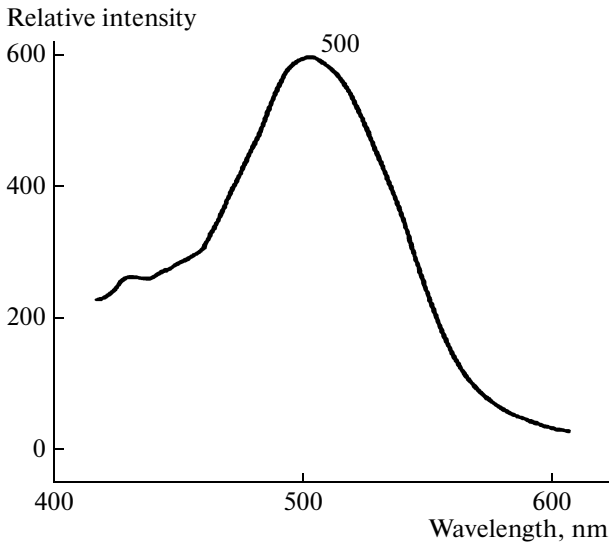

Fig. 6. Emission spectra of the sample prepared through gel technique.

tra. The excitation is at 304 and 321 nm, the emission spectra are at 500 nm. The excitation and emission energy of nano $SrAl_2O_4$: Eu, Dy are 3.835 and 2.480 eV respectively, while that of micron $SrAl_2O_4$ Eu, Dy are 3.444 and 2.384 eV. The authors provided a brief description of the luminescent mechanism of nano $SrAl_2O_4$ Eu, Dy. It is well known, because of the nanosize of the grain, the surface energy increases dramatically, which results in the distortion of atom structure and the change of the crystal field around Eu^{2+}. Although the 4*f* electron of Eu^{2+} is not sensitive to lattice environment because of the shielding function of the electrons in the inner shell, the 5*d* electron may be coupled strongly to the lattice. Consequently, the mixed states of 4*f*5*d* are splitted by the crystal field, as a result, some jumps, which are not allowed in micron $SrAl_2O_4$: Eu, Dy, can take effects in nano $SrAl_2O_4$: Eu, Dy and thus lead to the blue shift occurrence in the excitation and emission spectra. Figure 7 shows the decay curve of nano and micron $SrAl_2O_4$: Eu, Dy phosphor. The luminescent intensity of nano grade is found to be less than that of the micron grade. This also can be attributed to the surface energy. As for the mechanism of the long afterglow, it is the hole trapped transported-detrapped process that results in the properties of long afterglow of $SrAl_2O_4$: Eu, Dy phosphor, in which Dy ions play the role of a trapped energy level that can attract vacancies during the excitation and thus lower the initial luminescence and prolong the luminescent duration. From the point of view of energy level, it was suggested that the surface energy level was much deeper than the trap level of Dy and then attracts more vacancies than Dy, so that the initial luminescent intensity decreased greatly.

Comparative Study of Combustion Synthesis and Solid State Reaction Methods

Eu^{2+} and Dy^{3+} doped, green color emitting $SrAl_2O_4$ phosphor is considered as one of the best LLP materials. Until recent decade, SAO phosphors doped with Eu and Dy ions have attracted much attention since they show excellent properties [15]. Compared with classical sulfide phosphorescent phosphors, aluminates have several valuable properties [13] like high radiation intensity, color purity, longer afterglow, chemically stabilization, safe and no radioactivity, etc.

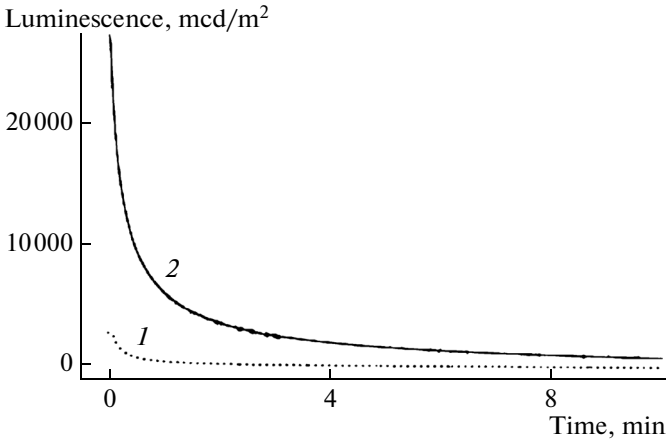

Fig. 7. Decay curves of nano (*1*) and micron (*2*) $SrAl_2O_4$: Eu, Dy phosphor.

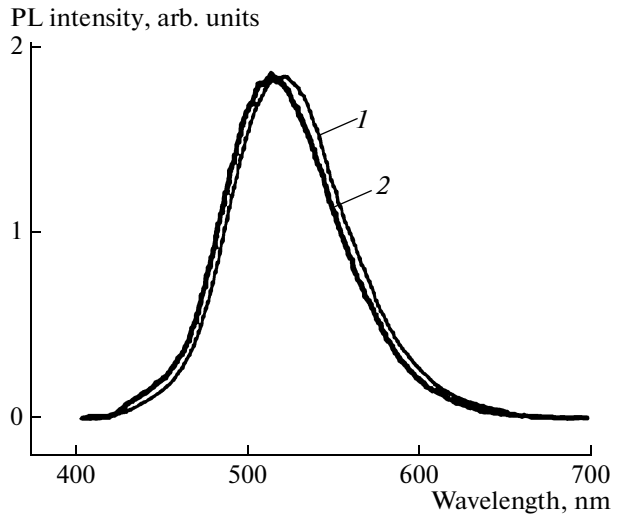

Fig. 8. PL spectra of $SrAl_2O_4$: Eu^{2+}, Dy^{3+} prepared by the solid state method (*1*) and the combustion method (*2*).

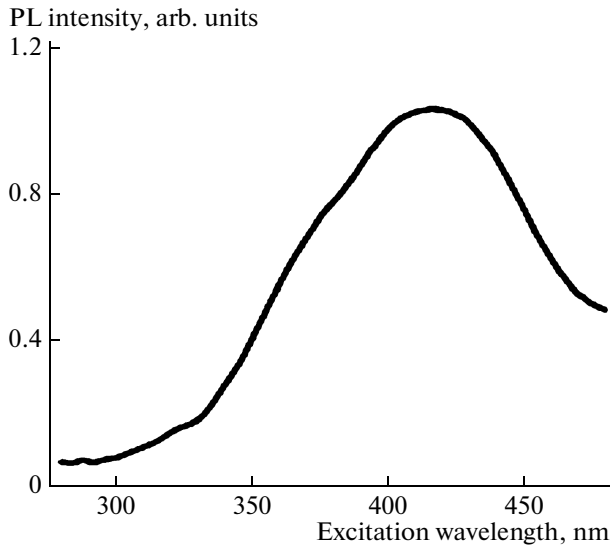

Fig. 9. Excitation spectrum of $SrAl_2O_4$: Eu^{2+}, Dy^{3+} phosphor prepared by combustion method ($\lambda_{em} = 516$ nm).

Together with the development of scientific technologies on materials, several chemical synthesis techniques, such as co-precipitation, sol–gel and combustion synthesis methods have been employed to prepare $SrAl_2O_4$: Eu^{2+}, Dy^{3+}. The combustion process to prepare powder phosphor is very facile and only takes few minutes. The $SrAl_2O_4$: Eu^{2+}, Dy^{3+} phosphor resulted from combustion method has improved but the sintering temperature of the sample is much lower than that prepared by solid state reaction or any other method.

Son et al. [31] described the Eu^{2+}, Dy^{3+} co-doped $SrAl_2O_4$ nanosized phosphorescent powder with high brightness and long afterglow prepared by urea-nitrate solution combustion method at 540°C for 5 min. The broad band PL of $SrAl_2O_4$: Eu^{2+}, Dy^{3+} was observed with maximum wavelength $\lambda_{max} = 516$ nm due to transitions from the $4f^6 5d$ to $4f^7$ configuration of the Eu^{2+} ions. The main peak of the emission spectrum shifted to the short wavelength compared with phosphorescence obtained by the solid state reaction method. The decay time of the afterglow for nanosized phosphorescence was observed to be shorter than that obtained by the solid state reaction method. The authors successfully illustrated the emission spectra of $SrAl_2O_4$: Eu^{2+}, Dy^{3+} at room temperature (RT) at excitation wavelength of 365 nm (Fig. 8). It consists of a broad band and the emission peak lying at 516 nm, which they attributed to the typical $4f^6 5d \longrightarrow 4f^7$ transition of Eu^{2+} ion [10]. The excitation spectrum at the emission wavelength 516 nm is shown at Fig. 9. It is noticed that the excitation spectrum has a broad band with the main peak at 410 nm. Compared with the phosphor resulted from solid state reaction method, the emission maxima of the phosphor prepared by the combustion method shifts to shorter wavelength (from 520 to 516 nm). This slight blue shift in the emission band was attributed to the changes of the crystal field around Eu^{2+}. Since the excited $4f^6 5d$ configurations of Eu^{2+} ion is extremely sensitive to the change in the lattice environment, the $5d$ electron may couple strongly to the lattice [21]. Hence, the mixed states of $4f$ and $5d$ configuration are splitted by the crystal field, which may lead to the blue shift of its emission peak. Figure 10 presents the decay times of $SrAl_2O_4$: Eu^{2+}, Dy^{3+} phosphors prepared by two techniques using the excitation wavelength 365 nm for 1 min. The rate of decay is comparatively faster in case of solid state reaction samples to those observed in the sample made by combustion method. The observed enhancement of afterglow intensity and lengthening of decay time of the sample by combustion method is attributed to increase in the number of defects due to rapid reaction combustion process and a higher concentration of Eu^{2+} generated in the process. Figure 11 illustrates the TL glow curve of $SrAl_2O_4$: Eu^{2+}, Dy^{3+} phosphor prepared by combustion method at a heating rate $\beta = 1$°C/s. The glow-curve of the sample shows a single peak at 86°C exhibiting the second order kinetics TL peak with activation energy ($E_a = 0.68$ eV) calculated by R. Chen method. It is seen that in $SrAl_2O_4$: Eu^{2+}, Dy^{3+} phosphor, Eu^{2+} and Dy^{3+} ions are represented by electrons and holes, respectively. It is the hole trapped-transported-detrapped process that results in the properties of long afterglow of $SrAl_2O_4$: Eu^{2+}, Dy^{3+} phosphor.

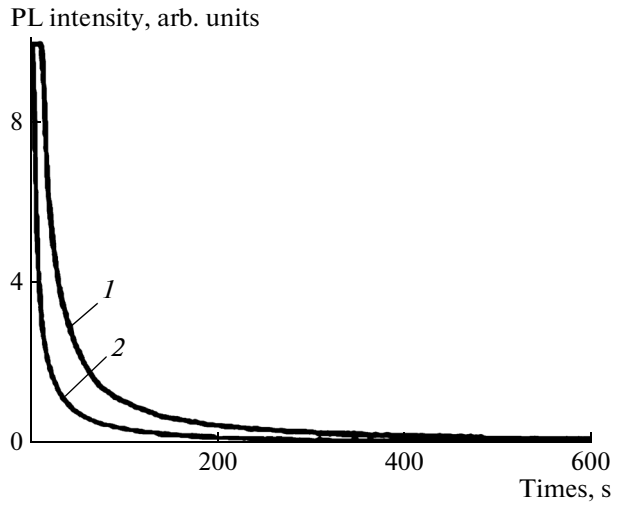

Fig. 10. The variation of PL intensity with time for $SrAl_2O_4$: Eu^{2+}, Dy^{3+} sample prepared by the (*1*) solid state reaction method, (*2*) combustion method.

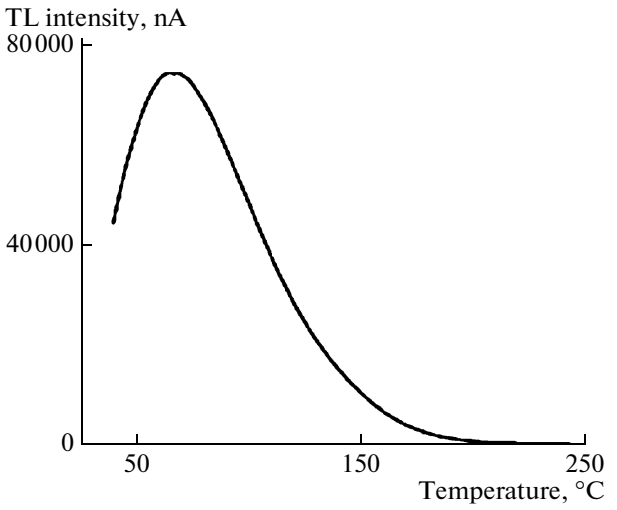

Fig. 11. TL glow curve of $SrAl_2O_4$: Eu^{2+}, Dy^{3+} sample.

Synthesis and LLP of Single-Crystal Nanosheets

Nanosheets can be regarded as a new class of materials possessing features such as single-crystalline quality, well defined chemical composition, and extremely high anisotropy with a nano-scale dimension [32]. The phosphors with nanosheet-shaped structure are quite intriguing because PL excitation energy is more effectively absorbed, ascribing to their large surface-to-volume ratios with respect to those of bulk materials. Furthermore, the morphology of nanosheets is suitable for fabricating optoelectronic devices such as electroluminescence (EL) panels, which consist of a stack of functional layers or sheets [33]. Till now, some nanosheets-based phosphors such as ZnS [34], YBO_3 : Eu^{3+} [35], $Bi_2SrTa_2O_9$ [36], $La_{0.90}Eu_{0.05}Nb_2O_7$ [37], $Eu_{0.56}Ta_2O_7$ [38], $La_{0.90}Sm_{0.05}Nb_2O_7$ [39] and their PL properties have been reported. However, the reports on phosphors nanosheets with LLP are few.

Xu et al. [40] synthesized single-crystal $SrAl_2O_4$: Eu^{2+}, Dy^{3+} nanosheets by a reliable two step method. The $SrAl_2O_4$: Eu^{2+}, Dy^{3+} nanosheets showed higher PL intensity (at 516 nm) as compared to corresponding commercial powders. Furthermore, the $SrAl_2O_4$: Eu^{2+}, Dy^{3+} nanosheets could sustain visible greenish-yellow light in dark places for more than 16 h, suggesting potential applications in many fields. Figure 12 presents the room temperature (RT) PL excitation and emission spectra of the $SrAl_2O_4$: Eu^{2+}, Dy^{3+} nanosheets (solid lines) and commercial $SrAl_2O_4$: Eu^{2+}, Dy^{3+} bulky powders obtained by solid-state reaction (dotted lines). The excitation spectrum of $SrAl_2O_4$: Eu^{2+}, Dy^{3+} nanosheets (monitored at 516 nm) shows three obvious sub-band peaks centered at about 396, 418, and 448 nm, clearly demonstrating the crystal field splitting of five-fold degenerate $5d$ excited level of Eu^{2+} ions. Under an excitation wavelength of 396 nm, the sample displays only one greenish-yellow broad band emission peak located around 516 nm. The bandwidth of peak is quite large (200 nm) but symmetric, indicating only one luminescent center corresponding to the $4f^6 5d \longrightarrow 4f^7$ ($^8S^{7/2}$) electric

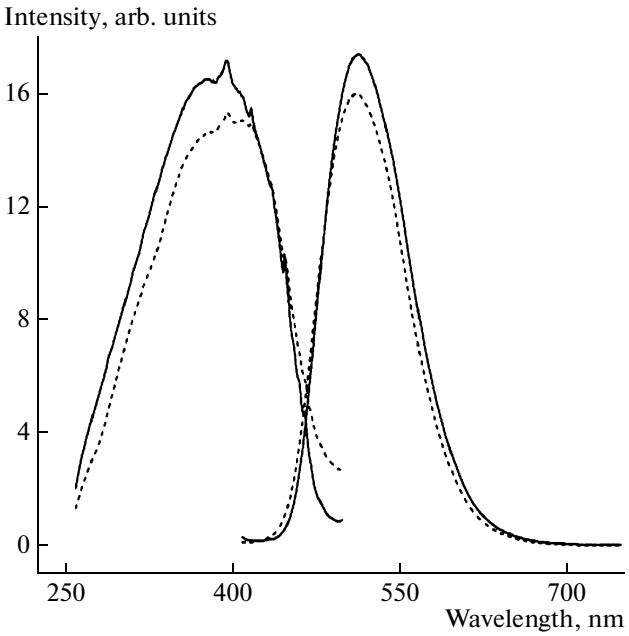

Fig. 12. PL excitation and emission spectra of the obtained $SrAl_2O_4$: Eu^{2+}, Dy^{3+} nanosheets (solid lines) and commercial $SrAl_2O_4$: Eu^{2+}, Dy^{3+} powders (dotted lines) at RT. See text for explanation.

dipole-allowed transition of Eu^{2+} [41]. The locations of excitation and emission peaks of $SrAl_2O_4$: $Eu^{2+}Dy^{3+}$ nanosheets are hardly changed, compared with commercial powders. However, the relative intensity of the excitation and emission peaks is enhanced. This point is of prime importance as above observation is different from previous reports on nanoparticles [41] and nanotubes of $SrAl_2O_4$: Eu^{2+}, Dy^{3+} [42].

For nanosized phosphors, the absorption of excitation light is reduced because of strong light scattering of nanocrystals and thus their emission strength is decreased. On the other hand, a lot of defects are easy to form on the surface of phosphors because of the high surface area of the nanometer powders prepared by common methods, which may result in the relatively less amount of luminescent centers in the host lattice available for direct radiation. Therefore, it results in the weaker fluorescence intensity. The authors explained the reasons why the $SrAl_2O_4$: Eu^{2+}, Dy^{3+} nanosheets exhibit stronger luminescent intensity than that of commercial bulky powders. First reason is the synthesized $SrAl_2O_4$: Eu^{2+}, Dy^{3+} nanosheets have good crystallinity, single crystal structure, and are free of defects. Secondly, the PL excitation energy is more effectively absorbed by nanosheet due to its large surface-to-volume ratio with respect to those of bulk materials. They demonstrated in Fig. 13 the decaying curves of $SrAl_2O_4$: Eu^{2+}, Dy^{3+} nanosheets and commercial counterpart at RT after the removal of the light excitation for about 30 s. The results indicate that the decaying processes of both the two kinds of phosphors contain' a rapid decaying process and a slow decaying one. However, the $SrAl_2O_4$: Eu^{2+}, Dy^{3+} nanosheets decayed more rapidly than commercial powders prepared by solid state reaction. The reason is that the synthesized nanosheets have good crystallinity, fewer defects in the inner phosphor, fewer crystallographic distortions, and shallower trap level than the phosphors obtained from solid state reaction method, so that the decay of afterglow is hastened. In addition, fast speed of hole mobility and electron–hole recombination in nanosheet with good crystallinity will decrease retrapping probability and further prompt the decay process [41].

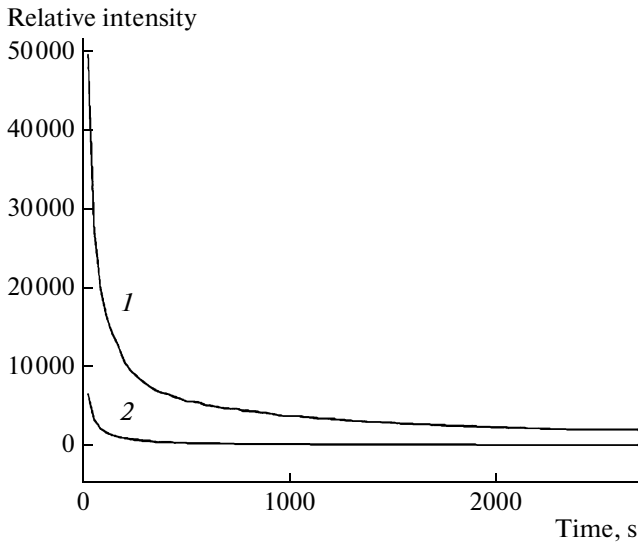

Fig. 13. Afterglow decay curves of $SrAl_2O_4$: Eu^{2+}, Dy^{3+} (*1*) nanosheets and (*2*) commercial counterpart at RT after the removal of the light excitation for 30 s.

The Influence of Processing Conditions on Host Crystal Structure

In recent years, $SrAl_2O_4$: Eu^{2+} phosphor has been widely studied as a long-persistent phosphor [43]. Many researchers have reported the influence of Eu^{2+} concentration on luminescent properties [44]. The emission from Eu^{2+} ions as emission centers in $SrAl_2O_4$: Eu^{2+}, Dy^{3+} phosphors strongly depend on the host lattice and can occur from ultraviolet to red region. This is because the excited $4f^65d$ configuration of Eu^{2+} is extremely sensitive to the change in the lattice environment of host structure [45].

Shafia et al. [46] reported the spectroscopic and host phase properties of Eu and Dy doped $SrAl_2O_4$ phosphors with a series of different initiating combustion temperature and urea concentration as a fuel. Initiating temperature higher than 600°C causes to increase the proportion of the hexagonal form. It is mentioned in some references that only the monoclinic phase of $SrAl_2O_4$ shows luminescence properties when doped with RE ions [47]. For investigation of the structural effect on the luminescence properties, the mass fraction ratio of the monoclinic phase is calculated theoretically. The 600°C temperature is confirmed as the best initiating combustion temperature with most fraction of monoclinic phase (MP) (Fig. 14). With increasing fuel concentration in stoichiometric sample ($f/o = 1$) the $SrAl_2O_4$ weak peaks are observed to be accompanied by impurity phase ($Sr_3Al_2O_6$). This result indicates that the heat released by combustion reaction is not enough to form the pure $SrAl_2O_4$ phase due to low adiabatic temperature. Higher concentration of fuel effective on the fraction of monoclinic shape of $SrAl_2O_4$ phase is shown in Fig. 15. Figure 16 presents the emission (a) and excitation (b) spectra of the stoichiometric samples with different urea concentration (0.5–3.5). The emission spectra show an asymmetrical broad band centered at 517 nm. This emission band corresponds to the $4f^65d$–$4f^7$ transition in Eu^{2+} ions, the $4f$–$5d$ transition in Eu^{2+} ions is an allowed one [48]. Figure 17 shows that when the ratio of urea is 2.5 times higher than theoretical content, the resulted $SrAl_2O_4$: Eu^{2+}, Dy^{3+} phosphors gave highest emission intensity.

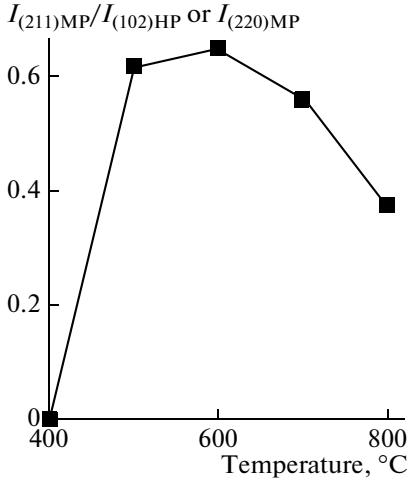

Fig. 14. Fraction of monoclinic phase variation by different initiating combustion temperature.

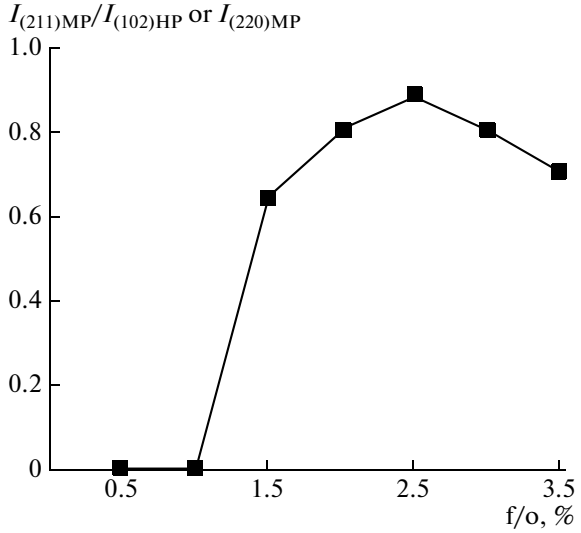

Fig. 15. Fraction of monoclinic phase variation by different concentration of fuel (urea).

Because a too high concentration of fuel releases higher heat that leads to increase in the adiabatic temperature of combustion, which is not favorable for forming the $SrAl_2O_4$ of single phase monoclinic structure and how observed in Fig. 15, the fraction of hexagonal phase became larger.

Effect of Trivalent RE Dopants on Optical Properties

Amongst different RE ions, Europium (Eu) is often employed by researchers for making red emitting phosphors where the prominent 612 nm emission band arises from electric dipole moment allowed transitions [49]. These properties have been observed in the following compounds: $SrAl_2O_4$: Eu^{2+}, Dy^{3+}, B^{3+} [50], $Sr_4Al_{14}O_{25}$: Eu^{2+}, Dy^{3+}, B^{3+} [51], $SrAl_4O_7$: Eu^{2+}, Dy^{3+} [52], $SrAl_{12}O_{19}$: Eu^{2+}, Dy^{3+}, $Sr_2A_{16}O_{11}$: Eu^{2+}, Dy^{3+} [53], $SrAl_2O_4$: Eu^{2+}, Dy^{3+} [54]. In addition to a higher chemical stability, the intensity and the duration of the phosphorescence are the parameters, which make it possible to envisage a continuous light emission during a whole night (10 h), hence greatly renewing interests in the phosphorescence phenomenon.

Ayvacikli et al. [55] reported Er^{3+} doped $SrAl_2O_4$ phosphor for the first time and studied the effects of Eu^{3+} doping on it. The excitation and emission spectra of Eu doped $SrAl_2O_4$ phosphors are shown in Figs. 18 and 19, respectively. The excitation spectrum consists of three bands centered at 250, 310 and 370 nm, respectively (Fig. 18). The band at 250 nm is attributed to ligand to metal charge transfer (LMCT) state from fully filled $2p$ orbitals of O^{2-} to partially filled $4f^7$ levels of Eu^{3+} [56]. The peak centre at 370 nm is due to the $4f$–$5d$ transition of Eu^{2+} ion. These results show that these compounds could be excited by ultraviolet and visible light. For the $5d$ electron, the splitting of energy levels is strongly affected by the crystal field, and it makes the $4f^65d$–$4f^7$ ($^8S_{7/2}$) transition of Eu^{2+} ion possible. The authors observed that the emission intensities increase with the increasing H_3BO_3, concentration. Actually, H_3BO_3 lowers the crystalline growth temperature and greatly promotes the reaction process. While adding more concentration of H_3BO_3 the presence of borate in vitreous state lowers the luminescence intensity. In the excitation spectra, a broad excitation band centered at 370 nm could be due to existence of intermediate trapping states (ITS). It is seen that the intensity of charge transfer transition at 250 nm is stronger than the 370 nm transition. The phenomenon is common because the typical Eu^{3+} activated phosphors show strong charge transfer transitions absorption band. Thus, it is anticipated that sufficient energy-transfer takes place between the host and the activator. Consequently, the emission spectrum of this sample was registered at 313 nm excitation wavelength. The resulting emission spectrum is depicted in Fig. 19. The intense peak at about 520 nm is associated with Eu^{2+} transitions [57] and indicates the presence of reduced europium in the sample. After excitation, the emission spectra are described by well-known $^5D_0$–^7F_J ($J = 0, 1, 2, 3...$) emission lines of the Eu^{3+} ion, with strong emission at 620 nm ($^5D_0$–$^7F_2$). In this case, the intermediate state is thought to populate the lowest $^5D_0$ state leading to the emission at 620 nm. Other emission bands were observed at 590, 650 and 700 nm. In absence of any inversion at RE ion site, the electric dipole transitions exist, and the maximum emission sensitive to the ligand environment is obtained at 650 nm. But, if 620 nm band is predominant, the magnetic dipole transition is predominant,

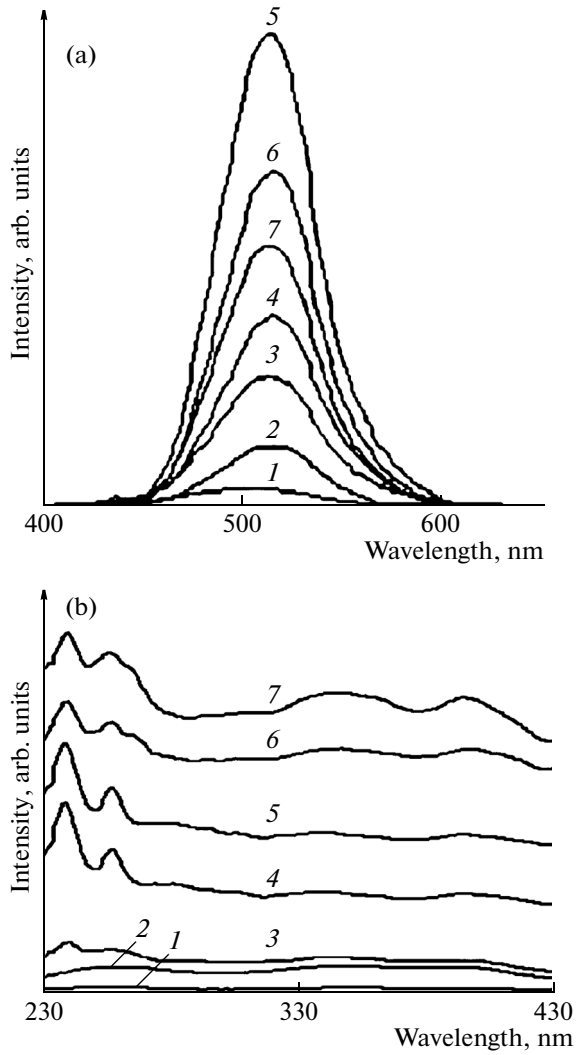

Fig. 16. Effect of the urea concentration on (a) the emission spectrum ($\lambda_{ex} = 254$ nm), (b) the excitation spectrum ($\lambda_{em} = 520$ nm): $f/o = 0.5$ (*1*), 1 (*2*), 1.5 (*3*), 2 (*4*), 2.5 (*5*), 3 (*6*), 3.5% (*7*).

which indicates that the Eu^{3+} ions lie in central symmetric sites.

Luminescence Enhancement of $SrO–Al_2O_3–B_2O_3$ (SAB) Glass Ceramics Using Femtosecond Laser

In the previous years, $Eu^{2+}Dy^{3+}$ co-doped phosphors have been widely studied as they exhibit high radiation intensity, long afterglow, high chemical stability, etc. [58]. For most of the research, the UV light has been used as the pump source to excite the luminescent materials. Presently, ultra-short pulsed femtosecond (fs) laser has attracted much attention due to the advantages of ultra-short interaction time, high electric field intensity, capability of modifying the internal structure without destroying the integrity of the glasses, high, peak power density, etc. [59].

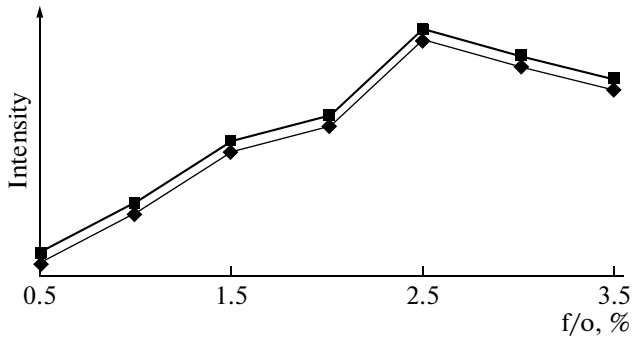

Fig. 17. Effect of fuel (urea) concentration on the luminescence properties: emission (flat line), excitation (thin line).

Zeng et al. [60] reported the spectroscopic investigation of Eu^{2+}/Dy^{3+} co-doped $SrO–Al_2O_3–B_2O_3$ (SAB) glass ceramic. The PL spectrum of the Eu^{2+}/Dy^{3+} co-doped SAB glass ceramic is illustrated in Fig. 20. As can be seen in the figure, two emission bands are visible. One of the bands is attributed to the spin-allowed transition of $4f^65d–4f^7$ ($^8S_{7/2}$) for the Eu^{2+} ions with the center at 515 nm, and other one is attributed to spin-forbidden transition of $^5D_0–^7F_2$ for the Eu^{3+} ions at 611 nm [61]. From excitation spectrum, it is evident that the Eu^{2+}/Dy^{3+} co-doped SAB glass ceramic can be effectively excited by UV light. As is well known, the $4f^65d–4f^7$ ($^8S_{7/2}$) transition of Eu^{2+} highly dependent on the crystal field symmetry [57]. In the $SrAl_2O_4$, the strontium chains consist of two different strontium sites, and are not perfectly linear [62]. Eu^{2+} ions in $SrAl_2O_4$ crystals occupy different Sr^{2+} sites, leading to a lower symmetry, which causes the splitting of the excited state. The emission spectrum of the Eu^{2+}/Dy^{3+} co-doped SAB glass ceramic is similar to that of $SrAl_2O_4$: Eu^{2+}, Dy^{3+} powder materials and gives a broad emission band but does not show any bands from Dy^{3+} ions. Such a phenomenon is ascribed to the existence of Dy^{3+} ions as traps in the structure [63]. Moreover, the presence of peak at 611 nm indicates that some Eu^{3+} ions could not be reduced to Eu^{3+} ions in the melting process or some Eu^{2+} ions were oxidized to Eu^{3+} ions when the melts were poured into the mold in air. The inset (a) of Fig. 20 shows a photograph of the sample irradiated by a 365 nm UV light.

Furthermore, it is important that the sample exhibits a high transmittance with green fluorescence. Figure 21 shows the emission spectra of Eu^{2+}/Dy^{3+} co-doped SAB glass/ceramic excited by an 800 nm fs laser and a 393 nm UV light, respectively. The spectral profile pumped by the near-IR fs laser is similar to that excited by the UV light, indicating that both of the emissions should come from the same origin (Eu^{2+}: Eu^{2+} : $4f^65d–4f^7$ ($^8S_{7/2}$)).

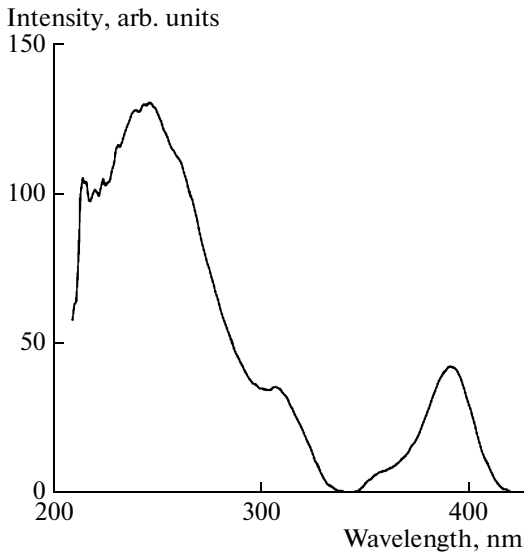

Fig. 18. PL excitation spectrum of Eu doped $SrAl_2O_4$.

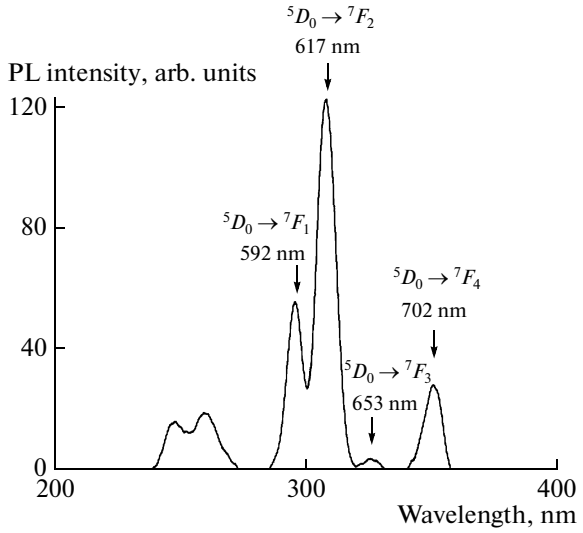

Fig. 19. PL emission spectrum of Eu doped $SrAl_2O_4$ taken with excitation at 234 nm.

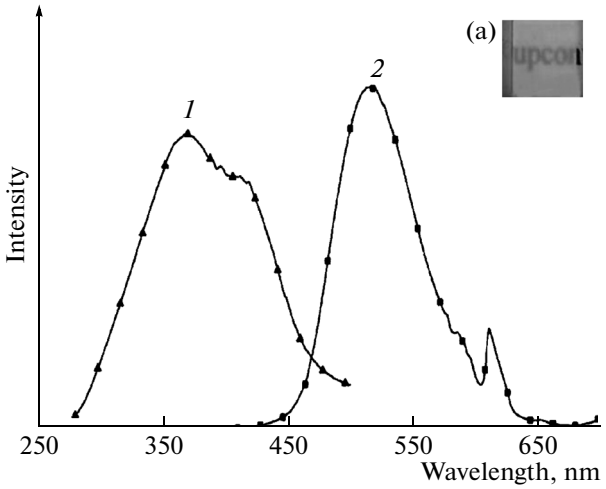

Fig. 20. Excitation (*1*, λ_{em} = 515 nm) and emission (*2*, λ_{ex} = 393 nm) spectra of the SAB glass ceramic. The inset (a) is a photograph of the SAB glass ceramic irradiated by a 365 nm UV light.

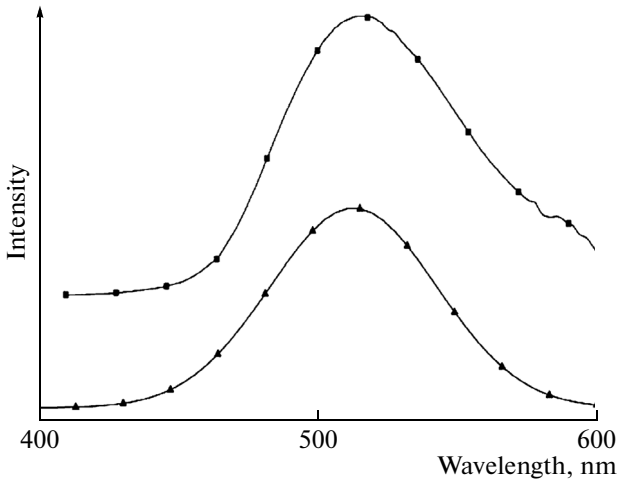

Fig. 21. Emission spectra of sample irradiated by a 800 nm fs laser (triangles) and a 393 nm UV light (squares).

Effect of UV-VIS Light on Optical Properties

The $SrAl_2O_4$: Eu^{2+}, Dy^{3+} is a phosphor characterized by a long persistent luminescence (PLUM) upon excitation with UV-VIS light and ionizing radiation. In this part of paper, we review the PLUM behavior as a function of beta irradiation dose in the 0–650 Gy range with a fixed dose rate of 5 Gy/min. The PLUM intensity shows a complex decay behavior, exhibiting a near linear response in the low dose range (0–1.7 Gy) and gradually increasing up to 160 Gy. The PLUM reached the saturation for higher doses (>275 Gy) with a slight decrease in the range of 300–650 Gy. In addition, a systematic PLUM enhancement was produced after a thermal cleaning procedure and irradiation at RT in a series of 10 cycles. The observed phenomenon may be related to a radiation-induced process of charge trapping accumulation, which is triggered by thermal stimulation during the irradiation stage. It improves the luminescent characteristics of $SrAl_2O_4$: Eu^{2+}, Dy^{3+} phosphors rendering them suitable for permanent display and illumination devices.

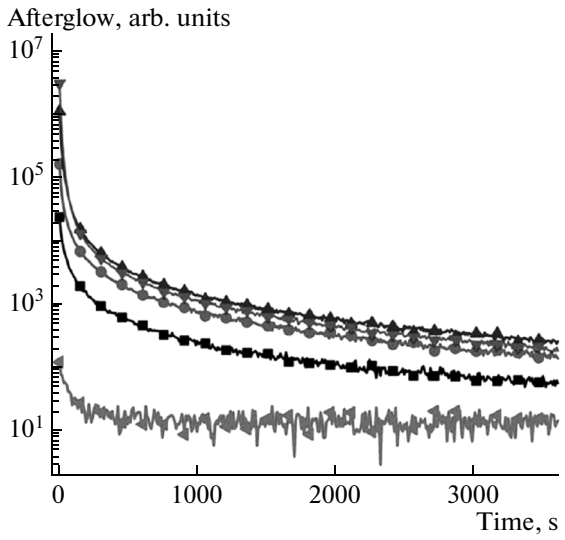

Fig. 22. Typical decay of the afterglow emission as a function of the UV-VIS light excitation: $\lambda_{ex} = 300$ (■), 350 (●), 400 (▲), 450 (▼), 500 nm (◄).

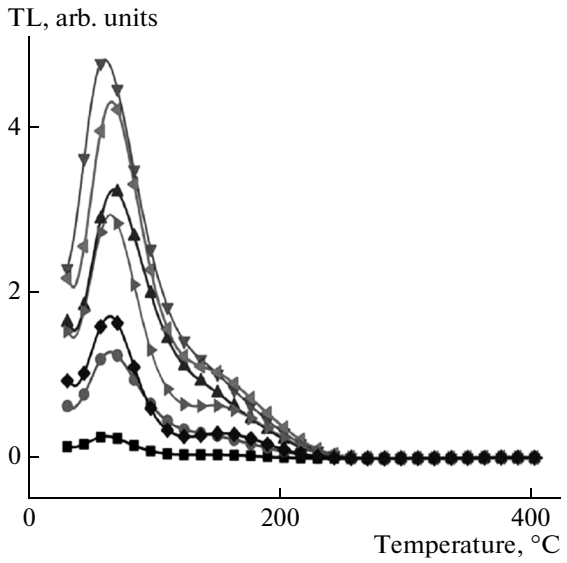

Fig. 23. Typical TL glow curve of $SrAl_2O_4$: Eu^{2+}, Dy^{3+} samples irradiated for 5 s with UV-VIS light in the range of 200–500 nm: $\lambda_{ex} = 300$ (■), 340 (●), 380 (▲), 400 (▼), 440 (◄), 480 (►), 500 nm (◆).

Earlier studies showed capability of $SrAl_2O_4$: Eu^{2+}, Dy^{3+} as beta [64] and UV radiation TL dosimeter [65]. It is referred for proper heating treatment and time delayed read out to control the PLUM decay signal. The $SrAl_2O_4$: Eu^{2+}, Dy^{3+} phosphor is adequate for ionizing radiation particularly in the 250–500 nm light excitation wavelength range which includes UVA (400–320 nm), UVB (320–290 nm) and UVC (290–200 nm) components of the solar electromagnetic spectrum of relevance to environmental and human health concern. A recent report has confirmed the TL excitation measurements on the $SrAl_2O_4$: Eu^{2+}, Dy^{3+} [27], therefore there is no doubt about the UV-VIS dose assessment performance of this phosphor in spite of its strong PLUM.

Pierre et al. [66] investigated the PLUM and TL properties of $SrAl_2O_4$: Eu^{2+}, Dy^{3+} phosphors excited with UV-VIS light in the 200–500 nm region. The decay of the PLUM is depicted in Fig. 22 showing a characteristic emission, which fades nonexponentially for the entire excitation wavelength from 300 to 510 nm. To further investigate the processes responsible for the PLUM in $SrAl_2O_4$: Eu^{2+}, Dy^{3+}, a series of TL glow curves above room temperature were obtained followed by excitation in the 200–580 nm range. The TL provides valuable insights about the trapping and detrapping processes related to the PLUM emission as illustrated in Fig. 23. The TL glow curve consists of a main peak around 70°C and a low-intensity TL band at 170°C. The broad band shape of the TL peaks suggests then being composed of several overlapped peaks or a multiple trapping level distribution. The TL read out shown in Fig. 23 was taken immediately after irradiation therefore the light output is overlapped with the PLUM emission. It accounts for the high TL emission at the start of the TL read out. Performing a TL read out starting 1 h after excitation, for which the 70°C low temperatures TL peak fades out, authors obtained a TL glow curve with a main peak at around 120°C, a low-intensity peak at 140°C, and a much lower intensity peak around 225°C. Therefore, the traps responsible for the main PLUM emission are at the lower temperature around 70°C. The trapping levels related to high-temperature TL band are certainly too deep to contribute to PLUM, at RT. This observation is consistent with afterglow studies of several PLUM, phosphors found in the literature. The PLUM occurred only if the stimulating radiation was in the 330–450 nm range as is shown in Fig. 24. Low intensity PLUM emission was observed around 330–370 nm and a high intensity broad band 370–475 nm with the intensity peaked around 420 nm. The PLUM emission spectrum is due to the Eu^{2+} transition between the $^8S_{7/2}$ ($4f^7$) ground state and the crystal field component of the excited $4f^65d$ configuration. The $SrAl_2O_4$: Eu^{2+}, Dy^{3+} phosphor also exhibited a TL excitation spectrum after stimulation with light of 200–500 nm wavelength shown in Fig. 24 with maxima at 380–400 nm. It is important to note that strong similarities are there between PLUM and TL excitation spectra. The PLUM and TL excitation spectra show a band maximum around 320–360 nm, which coincide with a TL excitation spectrum band maximum observed around the same wavelength range. Also, a maxima located

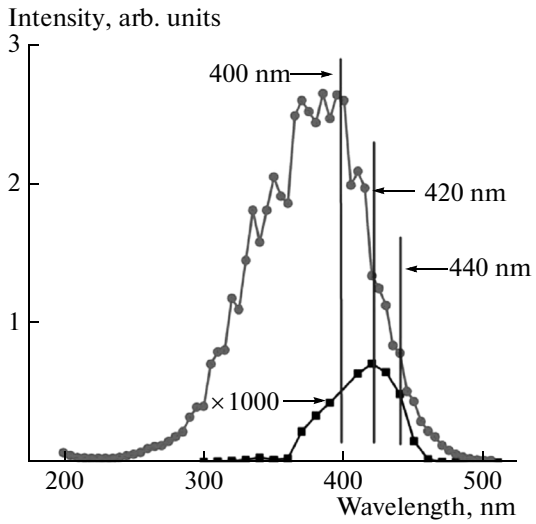

Fig. 24. PLUM (or afterglow, squares) and TL (circles) excitation spectra for UV-VIS irradiated $SrAl_2O_4$: Eu^{2+}, Dy^{3+} phosphor.

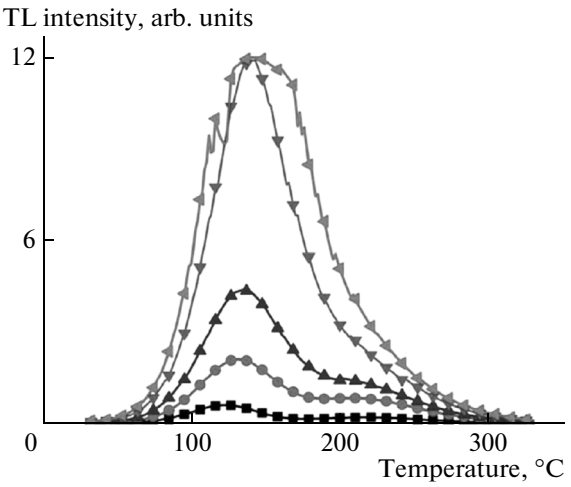

Fig. 25. TL glow curves of $SrAl_2O_4$: Eu^{2+}, Dy^{3+} phosphor at different irradiation time with light of 400 nm: 3 (■), 10 (●), 20 (▲), 60 (▼), 120 s (◀).

around 400 nm is observable for both the PLUM and TL excitation spectra, which may confirm that the PLUM and TL radiative emissions involve the same Eu^{2+} defect recombination center but with different efficiency. It is important to recall that the PLUM is mainly due to the radiative recombination of charge carriers at shallow trapping states after they are thermally released into the conduction (electrons) or valence (holes) band at RT. On the other hand, TL emission involves the radiative recombination of thermally stimulated detrapping of charge carriers trapped at shallow and deep traps. The TL glow curve displayed in Fig. 25 illustrates that determined number of charge carriers fill those deeper traps located around 125–150°C. Also, it indicates the involvement of trap filling process as a function of irradiation time exposure with light of 400 nm with a TL read out taken 1 h after irradiation to assure significant afterglow intensity decay.

Effects of Dopant Concentration on PL and TL Intensity

In our recent publication, PL emission spectra of $SrAl_2O_4$: Eu^{2+} at different volumes of Dy^{3+} by exciting the samples at a wavelength of 365 nm (Fig. 26) are reported [67, 68]. These spectra exhibit a broadband emission from Eu^{2+} accompanied by the peak at 515 nm, which is ascribed to the typical $4f^6 5d \longrightarrow 4f^7$ transitions of Eu^{2+}. There are no special emissions of Dy^{3+} and Eu^{3+} ions in the spectra, which imply that Eu^{3+} ions have changed to Eu^{2+} completely [69]. However, the position of the emission peak in the phosphorescence curve shows negligible change, regardless of the varied amount of the Dy^{3+} ions doping. Here the role of Dy^{3+} lies in inducing the formation of the holes trap level and in prolonging the afterglow. Thus, in $SrAl_2O_4$: Eu^{2+} samples with higher Dy^{3+} concentrations, creation of more and more hole-trap levels takes place leading to greater PL intensities [70]. This is corresponding to $4f^6 5d \longrightarrow 4f^7$ transition of Eu^{2+} ions. Although $4f$ electrons are not sensitive to the lattice environment due to the shielding effect of the electrons in the inner shell, the $5d$ electrons may

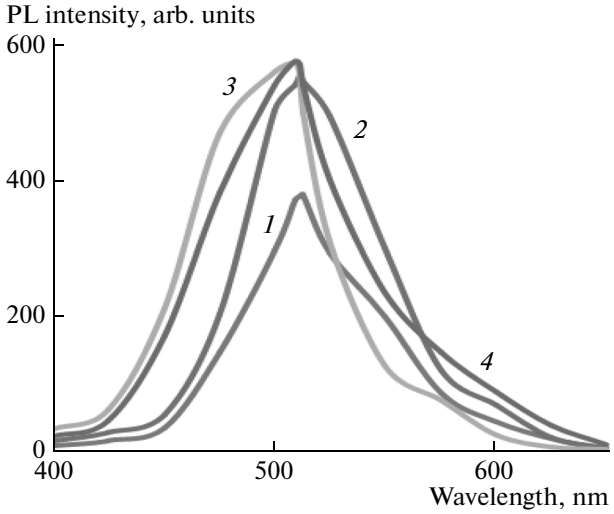

Fig. 26. Variation of PL intensity wavelength for $SrAl_2O_4$: Eu^{2+}, Dy^{3+} phosphor at different concentrations of Dy: $Sr_{0.99}Al_2O_4$: $Eu_{0.01}$ (*1*); $Sr_{0.98}Al_2O_4$: $Eu_{0.01}$, $Dy_{0.01}$ (*2*); $Sr_{0.97}Al_2O_4$: $Eu_{0.01}$, $Dy_{0.02}$ (*3*); $Sr_{0.96}Al_2O_4$: $Eu_{0.01}$, $Dy_{0.03}$ (*4*).

couple strongly to the lattice. As a result, the mixed states of $4f^6 5d$ are splitted by the crystal field and couple strongly to the lattice phonons [71].

The LLP oxide materials have been developed to replace the conventional sulfide afterglow materials because of their improved luminescent properties such as high initial brightness, long lasting time, suitable emission color and satisfactory chemical stability [68], which result in an unexpectedly large field of applications, e.g., luminous paints in highways, airports, buildings and ceramic products [72]. These oxide phosphors exhibit a long period of luminescence after an initial rapid attenuation, and the lasting time of this new kind of phosphors is more than 10 times than that of sulfide phosphors [73].

In another publication, we reported the TL glow curves for $SrAl_2O_4$: Eu, Dy powder phosphors prepared with $x = 0.01$, 0.02 and 0.03 ion doping of Dy^{3+} (Fig. 27) [74]. The general nature of TL curves is similar in different cases-each curve peaks at a temperature around 145°C. It is observed that varying concentration of Dy does not affect the peak position much. However, the emission intensity is found to increase with increasing Dy concentration and for $x = 0.02$ molar ratio, the intensity is quenched [75] and decreases for further concentration ($x = 0.03$). The reason for such quenching is the increase in probability of non-radiative transitions of the luminescent molecules from the excited state to the ground state in comparison to the probability of radiative transitions.

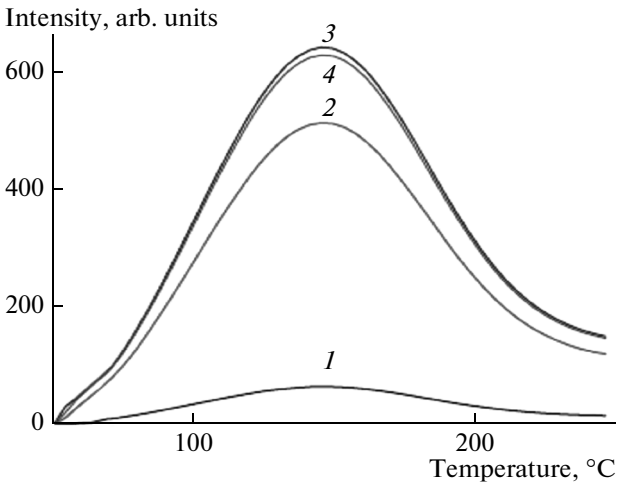

Fig. 27. TL glow curves of $SrAl_2O_4$: Eu phosphors with different Dy concentrations: the same as in Fig. 26.

FUTURE ASPECTS

On the basis of above discussion, it is for sure that persistent luminescent research has a promising future. However, since persistent luminescence is dependent upon both the interaction of localized levels of Eu^{2+} with extended conduction band states and the defect chemistry of a specific material (which is then dependent upon processing parameters), complete qualitative understanding of persistent luminescence is a goal for future study. A better understanding of the exact mechanism is crucial for the development of practical and commercial applications. However, many details are still unclear. At present, the mechanisms responsible for persistent luminescence are not yet fully understood. Most researchers agree on the general mechanism of charge carriers getting trapped in long-lived energy levels inside the band gap. The influence of co-dopants and lattice defects in the neighborhood of the activators are other unresolved issues. Various models have been proposed in the past few decades with only a small amount of experimental backup, but only recently researchers have started applying new and promising techniques that could confirm or disprove these theories. As is well established the emission and decay characteristics of the phosphors show improvement in their nano phase, it opens new avenues of research in this branch of material science. Little work has been carried out on the fabrication of technologically and practically important polynary complex nano tubes due to difficulty in their preparation and lot needs to be done. Commercial viability of the existing techniques is low due to costly capping agents and the difficulties faced in processing nano phosphors for display devices. There are two ways of further development. Firstly, the presently available methods should be improved, and secondly, new features should be added to match the future improvements of the PL and TL devices. In conclusion, this paper on the optical properties of RE doped strontium aluminate phosphors gives a brief but interesting overview of the state of the art in the research on persistent phosphors and offers many avenues for future research. Despite the relatively small size of the persistent phosphor research community, there is a strong drive toward the design and characterization of specific phosphors, the development of new application areas, and a more profound understanding of the trapping and release mechanisms.

ACKNOWLEDGMENTS

The authors are thankful to A.J.J. Bos, Zilong Tang, Nguyen Manh Son, Shao-Ming Huanga, Masoud Bodaghi, M. Barboza-Flores, N. Can, Danping Chen and their coworkers for permitting to review their works.

REFERENCES

1. P. F. Barbara, Acc. Chem. Res. **32**, 87 (1999).
2. G. B. Blasse and C. Grabmair, *Luminescent Materials* (Springer, Berlin, 1994).
3. A. S. Moskvin, E. V. Zenkov, and D. Panov, J. Lumin. **94**, 163 (2001).

4. R. K. Jain and R. C. Lind, J. Opt. Soc. Am. **73**, 47 (1983).
5. A. Henglein, Chem. Rev. **89**, 1861 (1989).
6. R. Rosetti, S. Nakahara, and L. E. Bras, J. Chem. Phys. **79**, 1086 (1983).
7. E. N. Harvey, *American Philosophical Society: Philadelphia, PA, USA*, 1957, vol. 44, p. 14.
8. W. Hoogenstraaten and H. A. Klasens, J. Electrochem. Soc. **100**, 266 (1953).
9. D. Wang, Q. Yin, Y. Li, and M. Wang, J. Lumin. **97**, 1 (2002).
10. T. Matsuzawa, Y. Aoki, N. Takeuchi, and Y. Murayama, J. Electrochem. Soc. **143**, 2670 (1996).
11. A. R. Schulze and H. M. Buschbaum, Anorg. Allg. Chem. **475**, 205 (1981).
12. H. Lange, US Patent **3**, 294 (1966).
13. G. Blasse and A. Bril, Philips Res. Rep. **23**, 201 (1968).
14. V. Abbruscato, J. Electrochem. Soc. **118**, 930 (1971).
15. W. Y. Jia, H. Yuan, L. Lu, H. Liu, and W. M. Yen, J. Cryst. Growth **200**, 179 (1999).
16. I. C. Chen and T. M. Chen, J. Mater. Res. **16**, 644 (2001).
17. J. Geng and Z. Wu, J. Mater. Synth. Proces. **10**, 245 (2002).
18. T. Aitasalo, J. Holsa, H. Jungner, M. Lastusaari, J. Niittykoski, M. Parkkinen, and R. Valtonen, Opt. Mater. **26**, 113 (2004).
19. C. Zhao and D. Chen, Mater. Lett. **61**, 3673 (2007).
20. T. Peng, L. Huajun, H. Yang, and C. Yan, Mater. Chem. Phys. **85**, 68 (2004).
21. J. Holsa, J. Hogne, M. Lastusaari, and J. Niittykoski, J. Alloys Comp. **323**, 326 (2001).
22. T. Aitasalo, J. Holsa, H. Jungner, M. Lastusaari, and J. Niittykoski, J. Alloy. Compd. **341**, 76 (2002).
23. Z. Qiu, Y. Zhou, M. Lu, A. Zhang, and Q. Ma, Acta Mater. **55**, 2615 (2007).
24. T. Katsumata, T. Nabae, K. Sasajima, S. Komuro, and T. Morikawa, J. Electrochem. Soc. **144**, L243 (1997).
25. R. Sakai, T. Katsumata, S. Komuro, and T. Morikawa, J. Lumin. **149**, 85 (1999).
26. P. Dorenbos, J. Electrochem. Soc. **152**, H107 (2005).
27. A. J. J. Bos, R. M. Duijvenvoorde, E. Kolk, W. Drozdowski, and P. Dorenbos, J. Lumin. **131**, 1465 (2011).
28. Z. Qi, C. Shi, M. Liu, D. Zhou, X. Luo, J. Zhang, and Y. Xie, Phys. Status Solidi A **201**, 3109 (2004).
29. H. Takasaki, S. Tananbe, and T. Hanada, J. Ceram. Soc. Jap. **104** (4), 322 (1996).
30. Z. Tang, F. Zhang, Z. Zhang, C. Huang, and Y. Lin, J. Europ. Cer. Soc. **20**, 2129 (2000).
31. N. M. Son, L. T. T. Vien, L. V. K. Bao, and N. N. Trac, J. Phys.: Conf. Ser. **187**, 012017 (2009).
32. T. G. Xu, C. Zhang, X. Shao, K. Wu, and Y. F. Zhu, Adv. Funct. Mater. **16**, 1599 (2006).
33. G. L. Frey, K. J. Reynolds, and R. H. Friend, Adv. Mater. **14**, 265 (2002).
34. C. H. Liang, Y. Shimizu, T. Sasaki, H. Umehara, and N. Koshizaki, J. Phys. Chem. B **108**, 9728 (2004).
35. X. C. Jiang, L. D. Sun, and C. H. Yan, J. Phys. Chem. B **108**, 3387 (2004).
36. S. Ida, C. Ogata, U. Unal, K. Izawa, T. Inoue, O. Altuntasoglu, and Y. Matsumoto, J. Am. Chem. Soc. **129**, 8956 (2007).
37. T. C. Ozawa, K. Fukuda, K. Akatsuka, Y. Ebina, and T. Sasaki, Chem. Mat. **19**, 6575 (2007).
38. T. C. Ozawa, K. Fukuda, K. Akatsuka, Y. Ebina, T. Sasaki, K. Kurashima, and K. Kosuda, Phys. Chem. C **112**, 1312 (2008).
39. T. C. Ozawa, K. Fukuda, K. Akatsuka, Y. Ebina, K. Kurashima, and T. Sasaki, J. Phys. Chem. **113**, 8735 (2009).
40. Y. F. Xu, D. K. Ma, M. L. Guan, X. A. Chen, Q. Q. Pan, and S. M. Huang, J. Alloys Comp. **502**, 38 (2010).
41. T. Y. Peng, H. P. Pu, X. L. Hu, B. Jiang, and Z. C. Yan, Mater. Lett. **58**, 352 (2004).
42. H. Yamada, W. S. Shi, and C. N. Xu, J. Appl. Crystallogr. **37**, 698 (2004).
43. E. Nakazawa and T. Mochida, J. Lumin. **72**, 236 (1997).
44. H. Song and D. Chen, Luminesc. **22**, 554 (2007).
45. S. H. Poort, W. P. Blokpoel, and G. Blasse, Chem. Mater. **7**, 1547 (1995).
46. E. Shafia, M. Bodaghi, and M. Tahriri, Curr. App. Phys. **10**, 596 (2010).
47. J. S. Benitez, A. D. Andres, M. Marchal, E. Cordoncillo, M. V. Regi, and P. Escribano, J. Sol. Chem. **171**, 273 (2003).
48. X. Yu, C. Zhou, X. He, Z. Peng, and S. Yang, Mater. Lett. **58**, 1087 (2004).
49. S. K. Sharma, S. S. Pitale, M. M. Mahk, M. S. Qureshi, and R. N. Dubey, J. Alloys Comp. **482**, 468 (2009).
50. F. Clabau, X. Rocquefelte, S. Jobic, P. Deniard, M. H. Whangbo, A. Garcia, and T. L. Mercier, Chem. Mater. **17**, 3904 (2005).
51. Y. Lin, Z. Tang, and Z. Zhang, Mater. Lett. **1**, 14 (2001).
52. C. Chang, D. Mao, J. Shen, and C. Feng, J. Alloys Comp. **348**, 224 (2003).
53. R. Zhong, J. Zhang, X. Zhang, S. Lu, and X. Wang, J. Lumin. **119–120**, 327 (2006).
54. P. J. R. Montes and M. E. G. Valerio, J. Lumin. **130**, 1525 (2010).
55. M. Ayvacikli, A. Ege, S. Yerci, and N. Can, J. Lumin. **131**, 2432 (2011).
56. Y. Pan, H. H. Y. Sung, H. Wu, J. Wang, X. Yang, M. Wu, and Q. Su, Mater. Res. Bull. **41**, 225 (2006).
57. H. Ryu and K. S. Bartwal, Physica B **404**, 1714 (2009).
58. A. Nag and T. R. N. Kutty, J. Alloys Comp. **354**, 221 (2003).
59. Y. Qiao, D. Chen, J. Ren, B. Wu, J. Qiu, and T. Akai, J. Appl. Phys. **103**, 023108 (2008).
60. H. Zeng, Z. Lin, Q. Zhang, D. Chen, X. Liang, Y. Xu, and G. Chen, Mater. Res. Bull. **46**, 319 (2011).
61. S. Liu, G. Zhao, H. Ying, J. Wang, and G. Han, Opt. Mater. **31**, 47 (2008).

62. S. H. Poort, W. P. Blokpoel, and G. Blasse, Chem. Mater. **7**, 1547 (2002).
63. B. Feng, J. Zhang, S. Li, and X. Yu, Am. Ceram. Soc. Bull. **87**, 53 (2008).
64. O. A. Tanori, R. Melendrez, M. P. Montero, B. Castaneda, V. Chernov, W. M. Yen, and M. B. Flores, J. Lumin. **28**, 173 (2008).
65. R. Melendrez, O. A. Tanori, M. P. Montero, W. M. Yen, and M. B. Flores, J. Lumin. **129**, 679 (2009).
66. C. P. Pierre, R. Melendrez, R. Garcia, M. P. Montero, and M. B. Flores, Rad. Measur. **46**, 1417 (2011).
67. D. S. Kshatri, A. Khare, and P. Jha, Optik - Int. J. Light and Electron Opt. **124**, 2974 (2013).
68. D. S. Kshatri and A. Khare, J. Alloys Comp. **588**, 488 (2014).
69. Y. H. Lin, Z. T. Zhang, F. Zhang, Z. L. Tang, and Q. M. Chen, Mater. Chem. Phys. **65**, 103 (2000).
70. K. V. D. Eeckhout, P. F. Smet, and D. Poehnan, Materials **3**, 2536 (2010).
71. C. Zhu, Y. Yang, G. Chen, S. Baccaro, A. Cecilia, and M. Falconieri, J. Phys. Chem. Sol. **68**, 1721 (2007).
72. Y. Murayama, N. Takeuchi, Y. Aoki, and T. Matsuzawa, US Patent, 1995, 5424006.
73. Y. L. Liu, B. F. Lei, and C. S. Shi, Chem. Mater. **17**, 2108 (2005).
74. D. S. Kshatri, A. Khare, and P. Jha, Chalcogenide Lett. **3**, 121 (2013).
75. G. C. Mishra, A. K. Upadhyay, S. K. Dwiwedi, S. J. Dhoble, and R. S. Kher, J. Mat. Sci. **47**, 2752 (2012).